Electronic Supplementary Information

Boosting the degradation of antibiotics via peroxymonosulfate activation with a Cu-based metal–organic framework

Ying Wu [a], Gang Liang [a], Wen-Bin Li [a], Xiao-Feng Zhong [a], Yang-Yang Zhang [a], Jia-Wen Ye [a], Tao Yang [a*], Zong-Wen Mo [a*], and Xiao-Ming Chen [b]

[a] *School of Environmental and Chemical Engineering, Jiangmen Key Laboratory of Synthetic Chemistry and Cleaner Production， Wuyi University, Jiangmen, Guangdong 529020, China;*

[b] *MOE Key Laboratory of Bioinorganic and Synthetic Chemistry, GBRCE for Functional Molecular Engineering, School of Chemistry, IGCME, Sun Yat-Sen University, Guangzhou 510275, China;*

[*] Corresponding author (Zong-Wen Mo and Tao Yang):

E-mail: wyuchemmzw@126.com; leoyanghit@126.com

1. EXPERIMENTAL SECTION

1.1. Reagents and Instruments.

All reagents and solvents were commercially purchased and used without further purification unless other noted. Elemental analysis (EA) was characterized with Perkin-Elmer 240 elemental analyzer. Thermogravimetric analyses were carried out on a NETZSCH TG209 F3 system under N_2 atmosphere with a heating rate of 10 ^{o}C min^{-1}. Powder X-ray diffraction (PXRD) data were collected using a Rigaku Mimi X-ray powder diffractometer (Cu-Kα) at room temperature with a scan speed of 10 ^{o} min^{-1}. The antibiotics concentrations were determined by high-performance liquid chromatography (HPLC) (Waters) equipped with a BEH C18 column (2.1 × 100 mm; 1.7 μm particle size). Electron paramagnetic resonance (EPR) experiments were performed on a Bruker instrument under ambient atmospheric condition (Bruker 216 EMX nano, Germany). The chemical state changes of C, O, and Cu before and after the catalyst reaction were analyzed by X-ray photoelectron spectroscopy.

1.2. Synthesis of $[Cu_3(\mu_3\text{-}O)(pypz)_3]NO_3$·guest (MAF-wyu2, 1).

A mixture of $Cu(NO_3)_2$·$4H_2O$ (2 mmol), 4-(1*H*-pyrazol-4-yl)pyridine (1 mmol), 1*H*-1,2,4-triazole (0.5 mmol) and *N,N*-dimethylacetamide (DMA, 50 mL) was stirred for 30 min, and then sealed in a 250-mL Teflon reactor and heated at 100 °C for 24 hours. After cooling to room temperature at a rate of 5 °C h^{-1}, dark blue cubic crystals were collected, washed with DMF, and dried in air. EA Calcd. (%) for $[Cu_3(\mu_3\text{-}O)(C_8H_6N_3)_3]NO_3$·$9(H_2O)$·$2.8(C_4H_9NO)$, $C_{35.2}H_{61.2}Cu_3N_{12.8}O_{13.8}$: C, 39.32; H, 5.74; N, 16.68. Found: C, 39.34; H, 5.63; N, 16.89.

1.3. Synthesis of MIL-53(Fe), MIL-101(Fe), $[Cu_3(\mu\text{-}OH)(pzca)_3(H_3O)]$, HKUST-1, MOF-74, FDM-6, Cu-MFU-4*l*, $[Cu_3(PyCA)_3]$.

These MOFs were synthesized based on the literature.[1-6]

1.4. The degradation of antibiotics experimental procedures.

All experiments were conducted at room temperature in 100 mL open beaker with a magnetic stirrer. 1.25 mg of the prepared sample was dispersed in 50 mL antibiotics solution (5 μmol L^{-1}) and distributed uniformly by sonication. The adsorption-

desorption equilibrium was reached by stirring the suspension solution for 30 min. Thereafter, PMS was added and stirred to ensure that the solution was mixed homogeneously. Meanwhile, the samples (1.0 mL suspension) were extracted and mixed with 10% hydroxylamine hydrochloride to stop the reaction at certain intervals. The sample was filtered through a 0.22 μm membrane and analyzed for SMX concentration by HPLC. The solutions with different pH are adjusted to the desired value by using $HClO_4$ or 0.10 mol L^{-1} NaOH. For the quenching experiments, methanol, ascorbic acid and furfuryl alcohol were added to the SMX-containing solution before the reaction. All experiments were replicated in triplicates.

1.5. Determination of PMS concentration.

The PMS concentration was estimated by a modified iodometric titration method. Firstly, a highly concentrated potassium iodide solution (KI, 0.50 mol L^{-1}) as well as a 50 mmol L^{-1} PMS solution was prepared. To dilute the PMS solution of 20 μL to 5 mL, and mixed 500 μL from the diluted PMS solution with 500 μL of 0.50 mol L^{-1} KI solution. After 10 min of reaction, the ultra-pure water was added and diluted to 5 mL, and the color-generating sample was detected at λ = 351 nm (UV-Vis spectrophotometer).

1.6. HPLC analysis.

Each sample was drawn 20 μL, injected and separated by the column with a flow rate of 0.30 mL min^{-1}. The mobile phase ratio of the various targets as follow:

Substrate	Mobile phase ratio (*v*:*v*)
sulfamethoxazole (SMX)	Methanol : 1‰ acetic acid = 60:40
oxytetracycline (OTC)	Acetonitrile : 1‰ acetic acid = 20:80
sulfamethazine (SMZ)	Methanol : 1‰ acetic acid = 60:40
ciprofloxacin (CIP)	Methanol : 1‰ acetic acid = 30:70
tetracycline (TC)	Methanol : 1‰ acetic acid = 80:20

1.7. EPR measurement.

5,5-Dimethyl-1-pyrroline *N*-oxide (DMPO) and 2,2,6,6-tetramethyl-4-piperidinol (TEMP) can be used as spin traps for the detection of free radicals in solution, respectively. Initially, DMPO-H_2O mixture, DMPO-MeOH mixture, and TEMP-H_2O

mixture were prepared. After that, 1 mL of suspension was extracted from the reaction solution with the catalyst, trapping agent and PMS at certain intervals (5 min, 15 min, 25 min) and the solution was aspirated with a quartz capillary to detect the spin-trapping adducts on an EPR spectrometer.

1.8 The degradation efficiency .

The degradation efficiency is the evolution of the substrate concentration over a given time interval and can be calculated by **eqn. S1**:

$$Efficiency\ (\%) = \frac{c_0 - c_t}{c_0} \times 100 \qquad \textbf{eqn. S1}$$

where C_0 and C_t are the concentrations of SMX at 0 min and at different time intervals, respectively.

1.9. Pseudo-first-order kinetics for SMX degradation.

The kinetic rates constant for SMX degradation is consistent with pseudo-first-order kinetics model, while the degradation rate of SMX can be calculated by **eqn. S2**:

$$\ln(\frac{c_t}{c_0}) = - k_{obs}t \qquad \textbf{eqn. S2}$$

where C_0 and C_t are the concentrations of SMX at 0 min and at different time intervals, respectively. k_{obs} denotes the pseudo-first-order kinetics constant rate (min^{-1}), while t is the reaction time.

1.10. The turnover number (TON) and turnover frequency (TOF).

The transformation efficiency for SMX at the active sites of MOF can expressed with TON, while this value can be calculated by **eqn. S3**:

$$TON = \frac{(Efficiency\ (\%))(Number\ of\ moles\ of\ substrate)}{Number\ of\ moles\ of\ catalyst} \qquad \textbf{eqn. S3}$$

TOF is the number of reaction cycles taking place in the established time intervals and can be calculated by **eqn S4**:

$$TOF = \frac{TON}{Time} \qquad \textbf{eqn. S4}$$

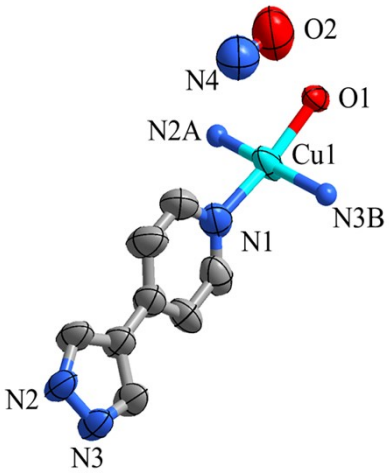

Fig. S1. The asymmetric unit of **1** (symmetry codes: A = 1/2-*x*, 1-*y*, 1/2+*z*; B = *x*, *y*, *z*).

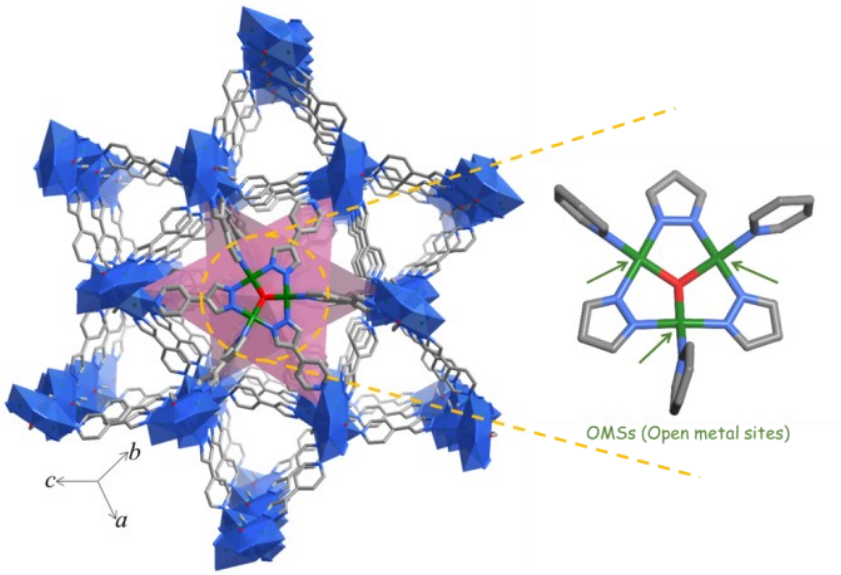

Fig. S2. The classic planar trinuclear $[Cu_3(\mu_3\text{-}O)]^{4+}$ cluster with exposed OMSs in **1**.

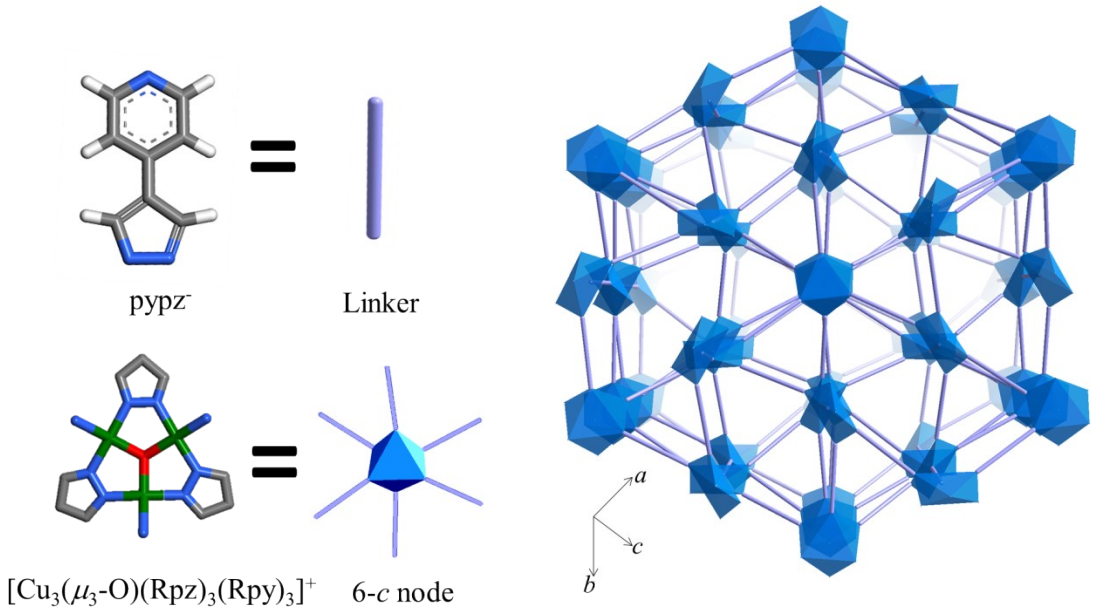

Fig. S3. The 6-connected topology network constructed by planar trinuclear $[Cu_3(\mu_3\text{-}O)]^{4+}$ clusters and $pypz^-$ ligands.

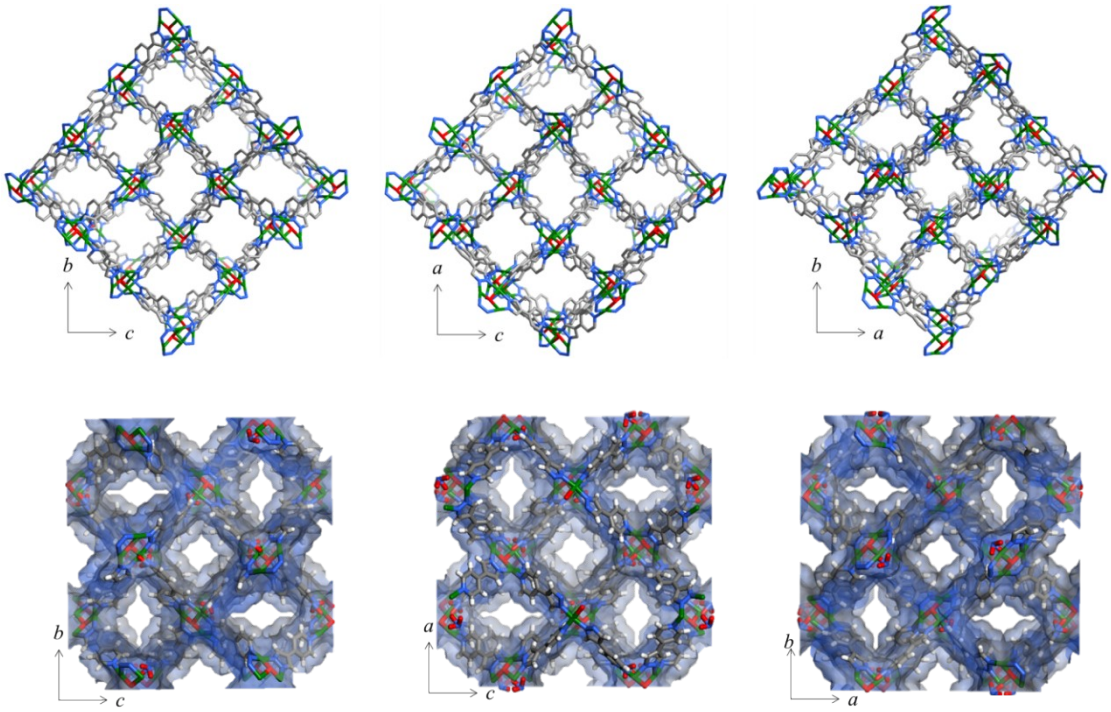

Fig. S4. The 3D coordination framework and pore surface structure of **1** along the *a*, *b*, *c*-axis, respectively.

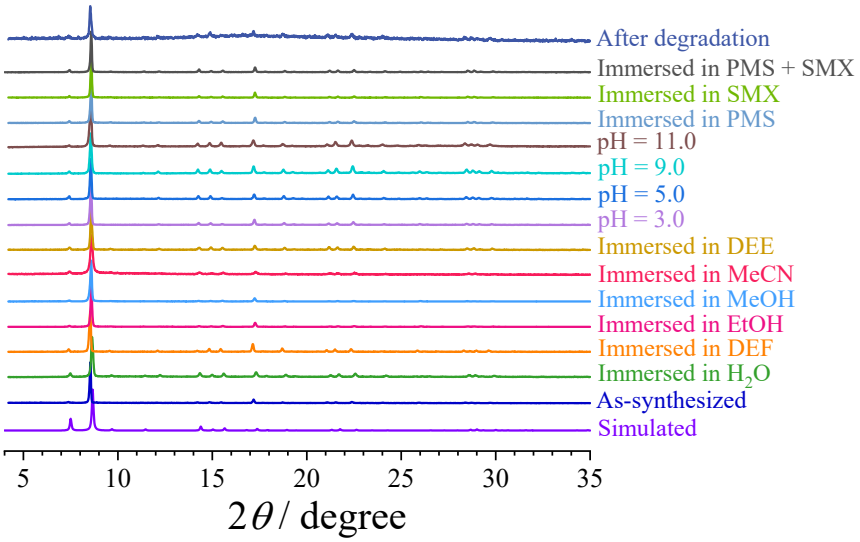

Fig. S5. PXRD patterns of **1** under various solvents.

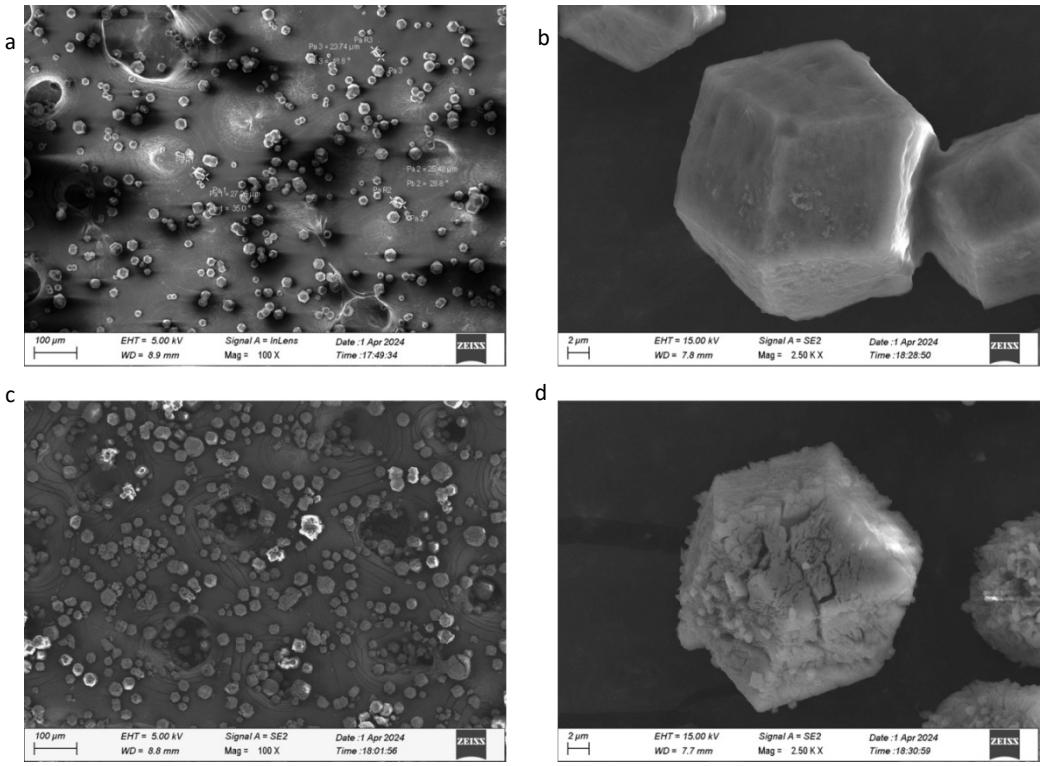

Fig. S6. The SEM images of **1** (a), (b) before and (c), (d) after the degradation.

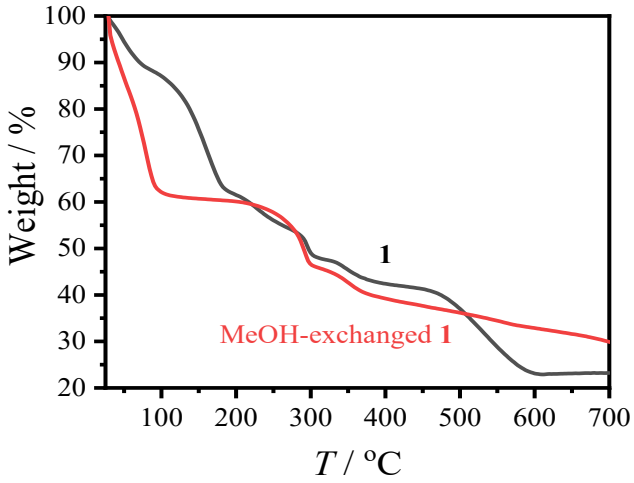

Fig. S7. Thermogravimetry curves of as-synthesized **1** and MeOH-exchanged **1**.

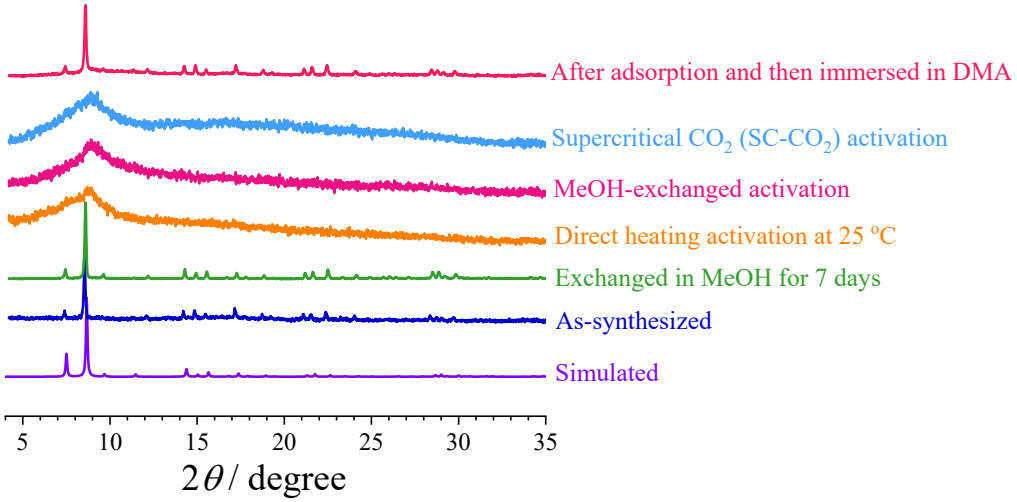

Fig. S8. PXRD patterns of activated **1** in various methods, and solvent soaking experiments.

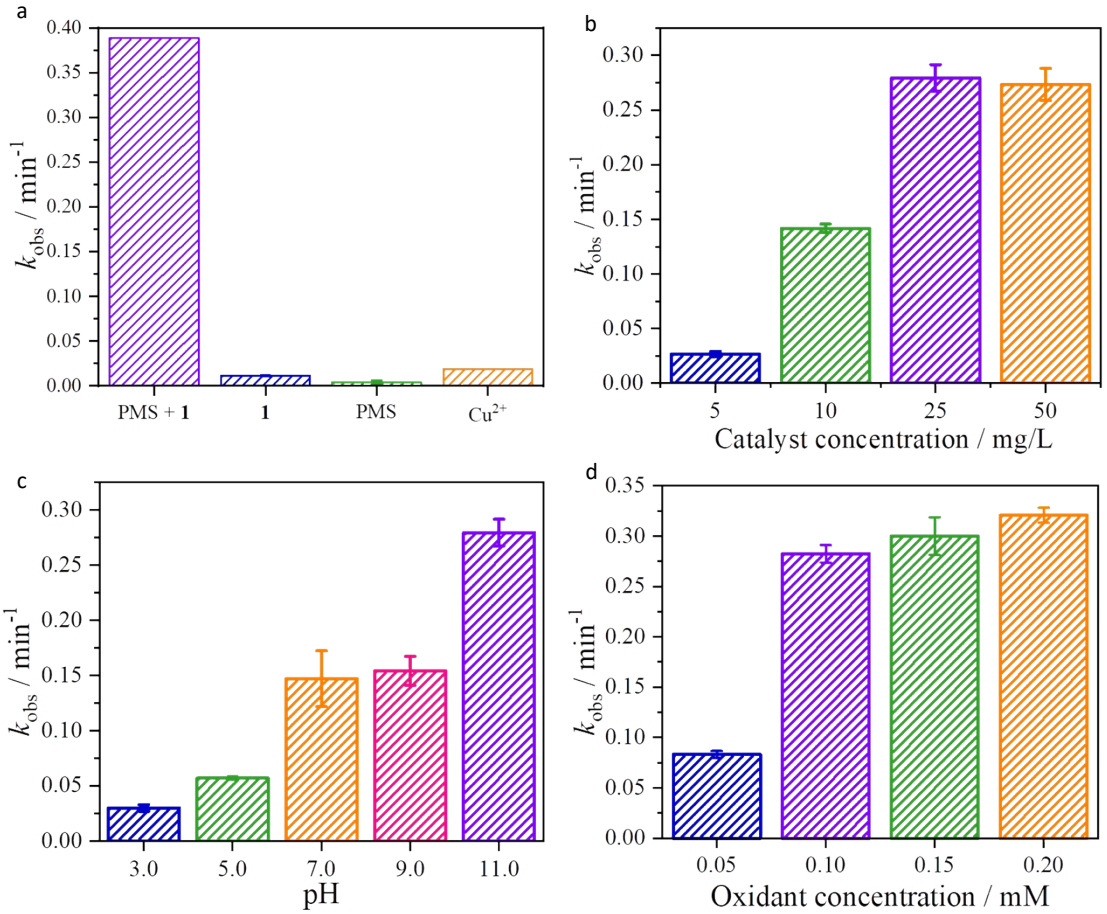

Fig. S9. (a) Degradation rates of SMX under different reaction systems. (Experimental conditions: pH = 7.0, SMX = 5 μM, Catalysts = 100 mg L^{-1}, pH = 11.0, Cu^{2+} = 100 mg L^{-1}, PMS = 100 μM, T = 25 °C). The influence of different reaction conditions of (b) catalyst concentration, (c) pH value, (d) oxidant concentration on SMX degradation rate. (Experimental conditions: pH = 11.0, SMX = 5 μM, Catalyst = 25 mg L^{-1}, PMS = 100 μM, T = 25 °C)

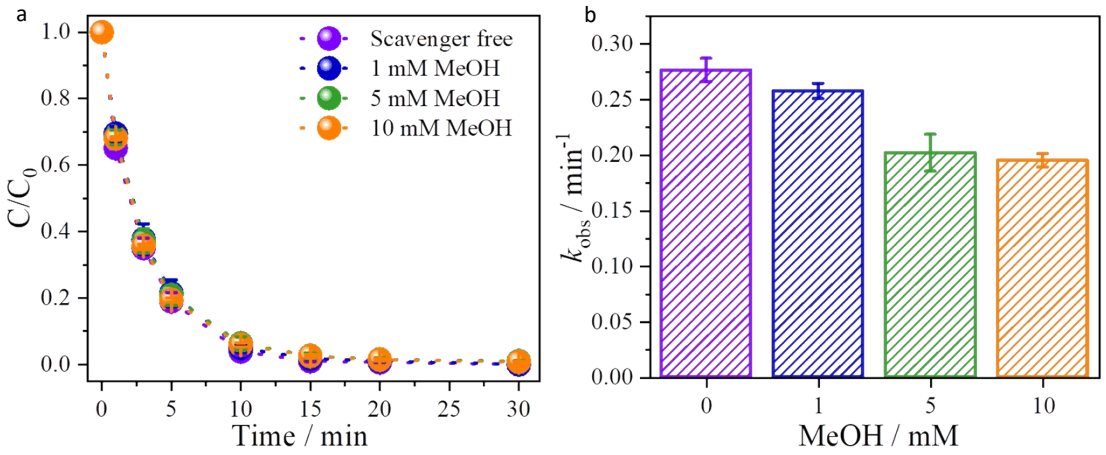

Fig. S10. MeOH quencher concentrations on (a) the SMX degradation efficiency, (b) the degradation rate. (Experimental conditions: pH = 11.0, SMX = 5 μM, Catalysts = 25 mg L^{-1}, PMS = 100 μM, T = 25 °C, MeOH = 1 mM, 5 mM, 10 mM)

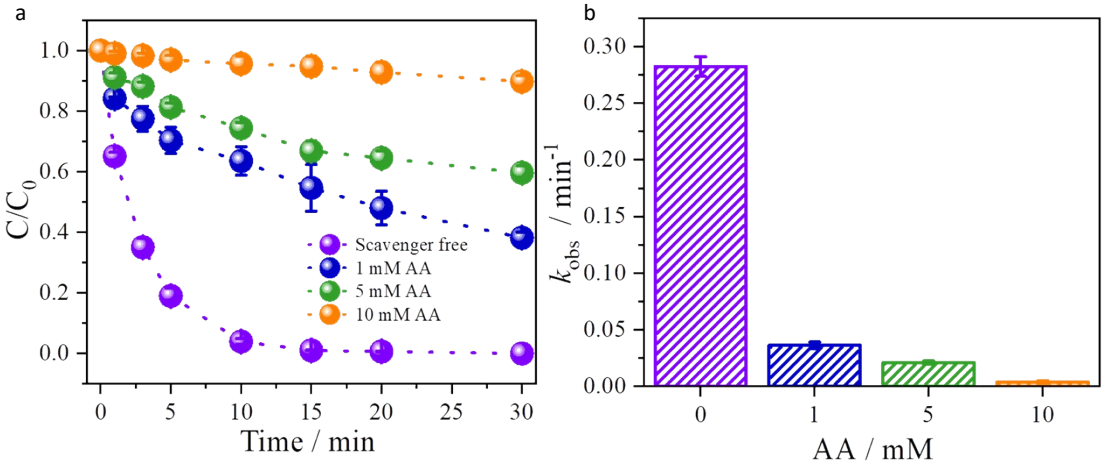

Fig. S11. AA quencher concentrations on (a) the SMX degradation efficiency, (b) the degradation rate. (Experimental conditions: pH = 11.0, SMX = 5 μM, Catalysts = 25 mg L^{-1}, PMS = 100 μM, T = 25 °C, L-ascorbic acid = 1 mM, 5 mM, 10 mM)

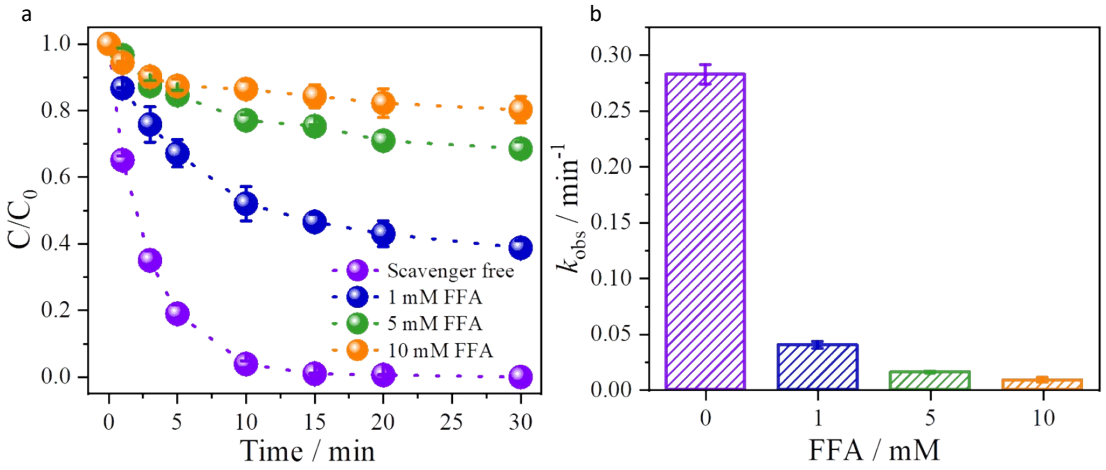

Fig. S12. FFA quencher concentrations on (a) the SMX degradation efficiency, (b) the degradation rate. (Experimental conditions: pH = 11.0, SMX = 5 μM, Catalysts = 25 mg L^{-1}, PMS = 100 μM, T = 25 °C, FFA = 1 mM, 5 mM, 10 mM)

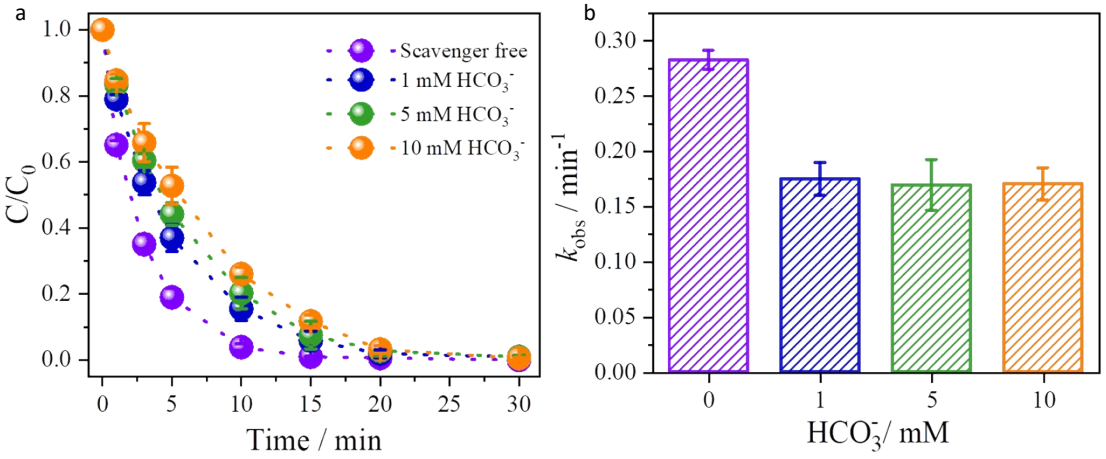

Fig. S13. (a) The degradation efficiency and (b) degradation rate of SMX at different HCO_3^- concentrations. (Experimental conditions: pH = 11.0, SMX = 5 μM, Catalysts = 25 mg L^{-1}, PMS = 100 μM, T = 25 °C, HCO_3^- = 1 mM, 5 mM, 10 mM)

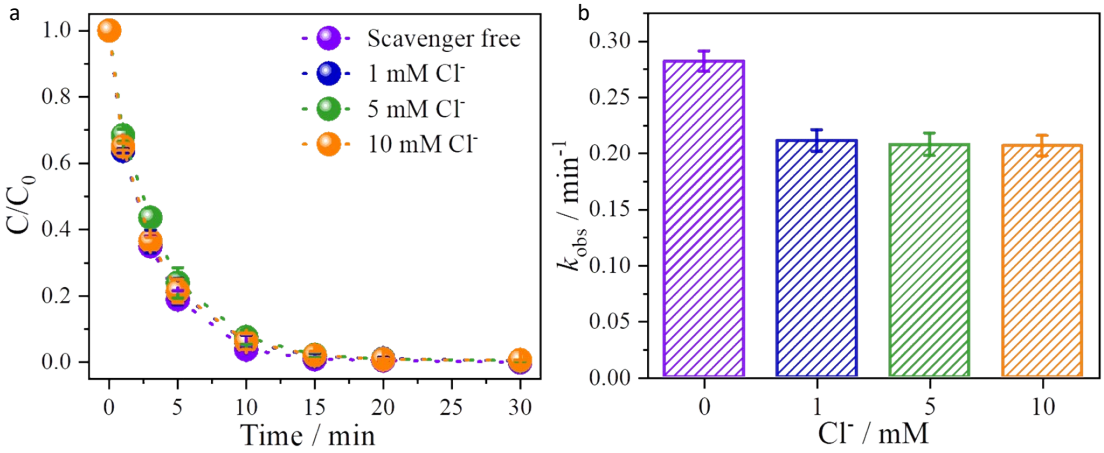

Fig. S14. (a) The degradation efficiency and (b) degradation rate of SMX at different Cl^- concentrations. (Experimental conditions: pH = 11.0, SMX = 5 μM, Catalysts = 25 mg L^{-1}, PMS = 100 μM, T = 25 °C, Cl^- = 1 mM, 5 mM, 10 mM)

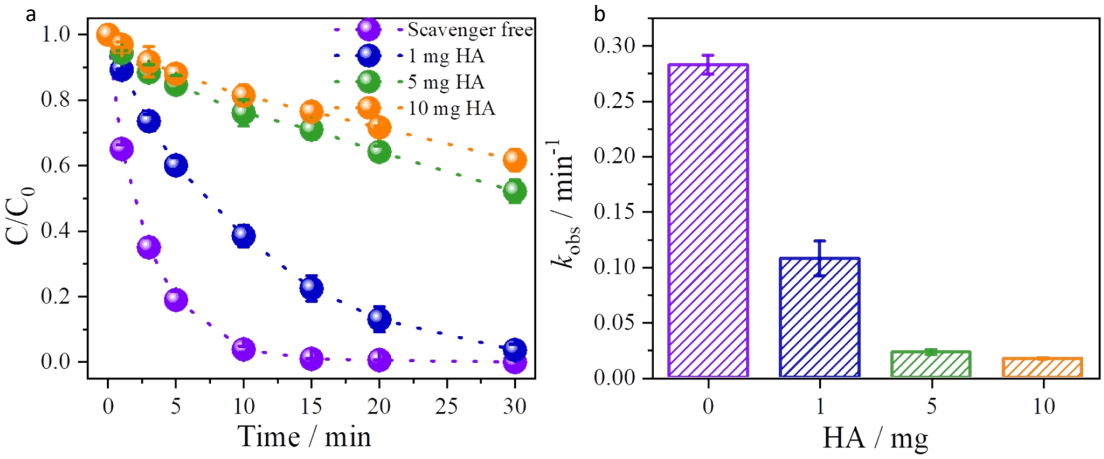

Fig. S15. (a) The degradation efficiency and (b) degradation rate of SMX at different HA concentrations. (Experimental conditions: pH = 11.0, SMX = 5 μM, Catalysts = 25 mg L^{-1}, PMS = 100 μM, T = 25 °C, HA = 1 mM, 5 mM, 10 mM)

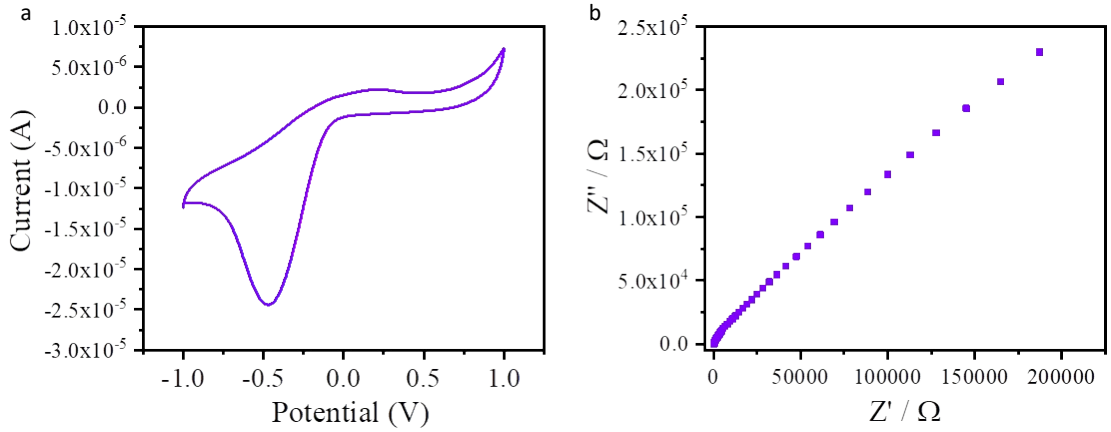

Fig. S16. (a) The cyclic voltammetry curve (CV) and (b) electrochemical impedance spectroscopy (EIS) of **1**.

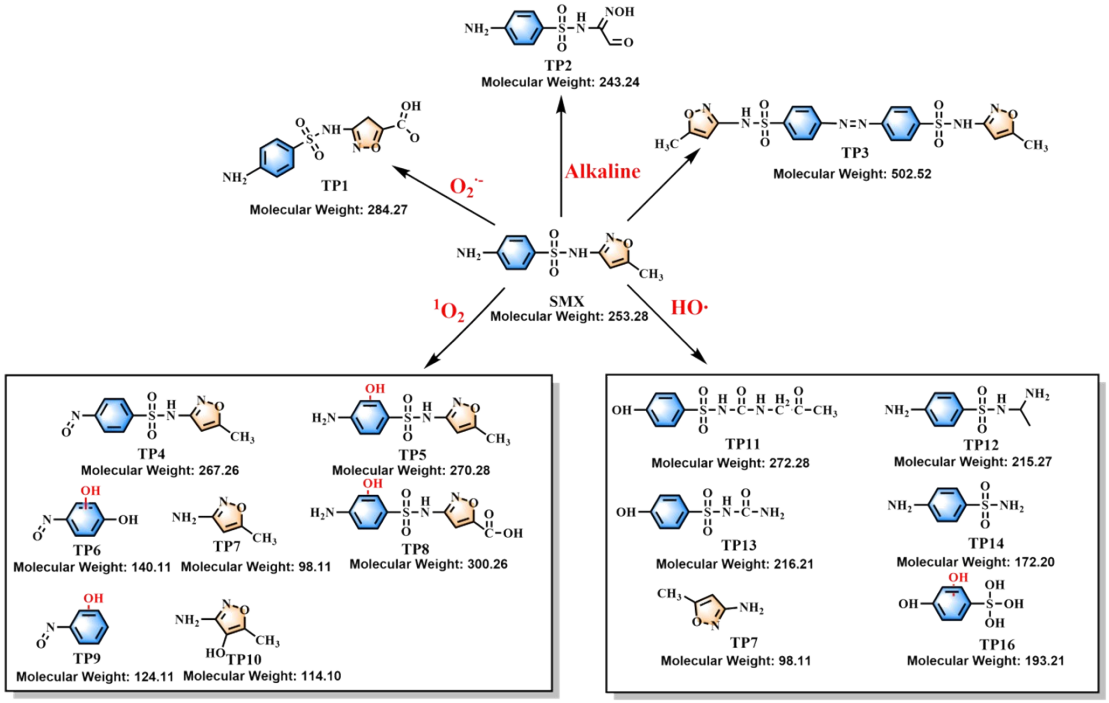

Fig. S17. The products/byproducts produced during the process of degradation.

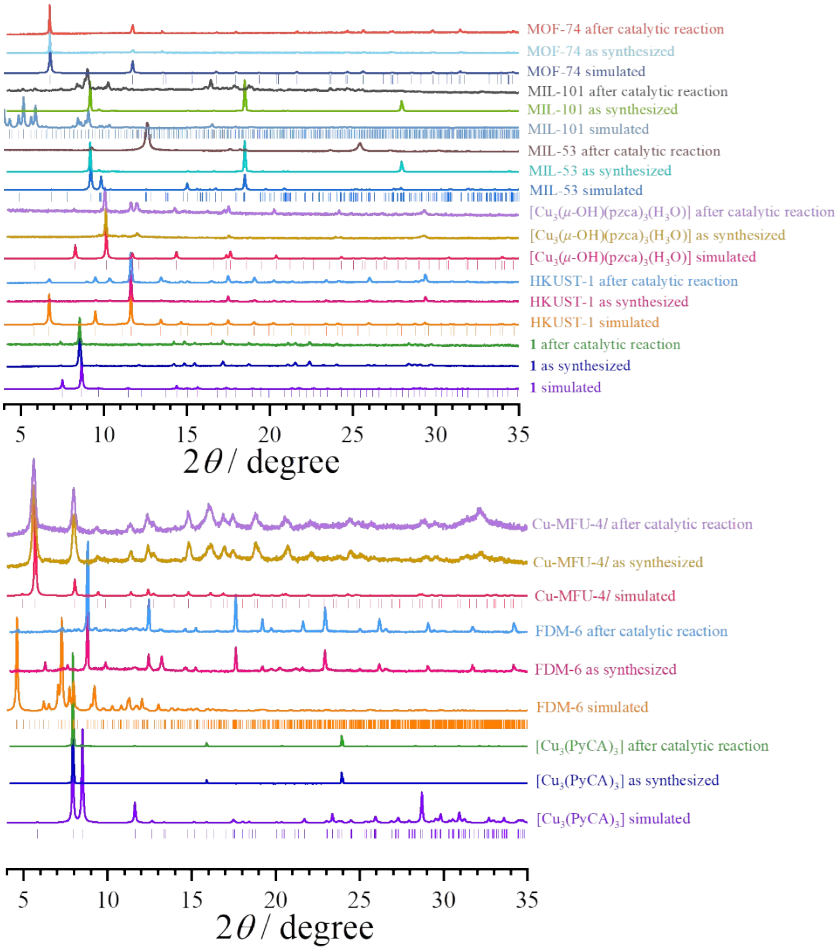

Fig. S18. PXRD patterns of **1** and other classical materials before and after the degradation.

Table S1. Crystallographic data and structural refinement details of **1**.

Complex	**1**
Formula	$C_{24}H_{18}Cu_3N_{10}O_2$
Formula weight	669.10
Temperature (K)	298(2)
Crystal system	cubic
Space group	*I*-43*d*
a/Å	28.8469(4)
b/Å	28.8469(4)
c/Å	28.8469(4)
α/°	90
β/°	90
γ/°	90
V/Å^3	24004.8(10)
Z	16
D_c /g cm^{-3}	0.741
reflns coll.	13693
unique reflns	3830
R_{int}	0.0408
R_1 [$I > 2\sigma(I)$][a]	0.0289
wR_2 [$I > 2\sigma(I)$][b]	0.0601
R_1 (all data)	0.0396
wR_2 (all data)	0.0634
GOF	0.884

[a] $R_1 = \Sigma||F_o|-|F_c||/\Sigma|F_o|$.

[b] $wR_2 = \{\Sigma w[(F_o)^2-(F_c)^2]^2/\Sigma w[(F_o)^2]^2\}^{1/2}$

Table S2. Comparison of degradation performances of **1** and other materials.

	Catalyst concentration	pH value	Oxidant concentration (PMS/PDS)	SMX	Reaction time (min)	Degradation efficiency (%)	Rate constant (min^{-1})	Ref.
1	25 mg L^{-1}	11.0 9.0 7.0	0.10 mM	5 μM	30 30 30	100.00 97.98 97.89	0.282 0.154 0.147	This work
MIL-88B(NH_2)(Fe)	1.0 g L^{-1}	5.0	1 g L^{-1}	10 mg L^{-1}	120	95	0.0216	7
Fe@C-800	0.4 g L^{-1}	ambient pH	PDS (0.2 mM)	10 mg L^{-1}	180	100.00	0.074	8
SA-Cu/rGO	0.1 g L^{-1}	6.0	0.4 g L^{-1}	10 mg L^{-1}	60	99.60	0.088	9
$LaMnO_3$-Cu-3	0.2 g L^{-1}	7.0	1.3 mM	19.76 μm	20	100.00	0.200	10
CuCo-HT	1.0 g L^{-1}	7.0	0.15 mM	0.1 mM	40	97.60	0.098	11
CuO@FeO_x@Fe_0	1.0 g L^{-1}	5.7	0.2 mM	10 mg L^{-1}	10	86.80	0.212	12
$CoFeO_{2.5}$	0.2 g L^{-1}	7.0	0.4 mM	40 μm	60	100.00	0.151	13
Co-NP	50 mg L^{-1}	6.4	0.15 mM	2.5 mg L^{-1}	60	88.00	0.034	14
NRGO	0.5 g L^{-1}	3.4	0.8 mM	0.04 mM	240	91.70	0.010	15
DMDB-800	1.0 g L^{-1}	5.56	2.5 mM	15 mg L^{-1}	60	90.20	0.025	16
N, S-BC	0.2 g L^{-1}	5.4	0.8 mM	20 μm	60	91.32		17
Co_3O_4@NPC/rGO	20 mg L^{-1}	7.0	0.2 mM	25 mg L^{-1}	10	100	0.3315	18

Table S3. Comparison of degradation performances of **1**, classical planar trinuclear $[Cu_3(\mu_3\text{-}O)]^{4+}$ clusters and MOFs under the same conditions. (Experimental conditions: pH = 11.0, SMX = 5 μM, Catalysts = 25 mg L^{-1}, PMS = 100 μM, T = 25 °C)

	Degradation efficiency (%)	Rate constant (min^{-1})	TON	TOF (min^{-1})
1	100.00	0.282	0.038	0.008
$[Cu_3(\mu\text{-}OH)(pzca)_3(H_3O)]$	71.11	0.043	0.005	0.001
HKUST-1	70.60	0.047	0.012	0.002
MIL-53(Fe)	25.13	0.011	0.005	0.001
MIL-101(Fe)	23.78	0.010	0.009	0.002
MOF-74	23.34	0.012	0.005	0.001
FDM-6	59.30	0.039	0.028	0.006
Cu-MFU-4*l*	71.68	0.053	0.036	0.007
$[Cu_3(PyCA)_3]$	83.45	0.059	0.008	0.002

Reference

1 P. Horcajada, C. Serre, G. Maurin, N. A. Ramsahye, F. Balas, M. Vallet-Regí, M. Sebban, F. Taulelle and G. Férey, Flexible porous metal-organic frameworks for a controlled drug delivery, *J. Am. Chem. Soc.*, 2008, **130**, 6774-6780.

2 K. M. L. Taylor-Pashow, J. Della Rocca, Z. G. Xie, S. Tran and W. B. Lin, Postsynthetic Modifications of Iron-Carboxylate Nanoscale Metal-Organic Frameworks for Imaging and Drug Delivery, *J. Am. Chem. Soc.*, 2009, **131**, 14261-+.

3 S. Q. Su, Y. B. Zhang, M. Zhu, X. Z. Song, S. Wang, S. N. Zhao, S. Y. Song, X. G. Yang and H. J. Zhang, An active-site-accessible porous metal-organic framework composed of triangular building units: preparation, catalytic activity and magnetic property, *Chem. Commun.*, 2012, **48**, 11118-11120.

4 B. B. Tu, Q. Q. Pang, H. S. Xu, X. M. Li, Y. L. Wang, Z. Ma, L. H. Weng and Q. W. Li, Reversible Redox Activity in Multicomponent Metal-Organic Frameworks Constructed from Trinuclear Copper Pyrazolate Building Blocks, *J. Am. Chem. Soc.*, 2017, **139**, 7998-8007.

5 P. Y. You, K. M. Mo, Y. M. Wang, Q. Gao, X. C. Lin, J. T. Lin, M. Xie, R. J. Wei, G. H. Ning and D. Li, Reversible modulation of interlayer stacking in 2D copper-organic frameworks for tailoring porosity and photocatalytic activity, *Nat. Commun.*, 2024, **15**, 11.

6 D. Denysenko, M. Grzywa, J. Jelic, K. Reuter and D. Volkmer, Scorpionate-Type Coordination in MFU-4*l* Metal-Organic Frameworks: Small-Molecule Binding and Activation upon the Thermally Activated Formation of Open Metal Sites, *Angew. Chem.-Int. Edit.*, 2014, **53**, 5832-5836.

7 J. Sun, J. Q. Wan, Y. Wang, Z. C. Yan, Y. W. Ma, S. Ding, M. Tang and Y. C. Xie, Modulated construction of Fe-based MOF via formic acid modulator for enhanced degradation of sulfamethoxazole:Design, degradation pathways, and mechanism, *J. Hazard. Mater.*, 2022, **429**, 128299.

8 M. J. Pu, J. Q. Wan, F. Z. Zhang, M. L. Brusseau, D. Q. Ye and J. F. Niu, Insight into degradation mechanism of sulfamethoxazole by metal-organic framework derived novel magnetic Fe@C composite activated persulfate, *J. Hazard. Mater.*, 2021, **414**, 125598.

9 F. Chen, X. L. Wu, L. Yang, C. F. Chen, H. J. Lin and J. R. Chen, Efficient degradation and mineralization of antibiotics via heterogeneous activation of peroxymonosulfate by using graphene supported single - atom Cu catalyst, *Chem. Eng. J.*, 2020, **394**, 124904.

10 P. P. Gao, X. K. Tian, W. Fu, Y. X. Wang, Y. L. Nie, C. Yang and Y. Deng, Copper in $LaMnO_3$ to promote peroxymonosulfate activation by regulating the reactive oxygen species in sulfamethoxazole degradation, *J. Hazard. Mater.*, 2021, **411**, 125163.

11 J. Wang, Q. Gong, J. Ali, M. Shen, J. Y. Cai, X. Q. Zhou, Z. W. Liao, S. L. Wang and Z. Q. Chen, pH-dependent transformation products and residual toxicity evaluation of sulfamethoxazole degradation through non-radical oxygen species involved process, *Chem. Eng. J.*, 2020, **390**, 124512.

12 Y. L. He, J. L. Zhang, H. Y. Zhou, G. Yao and B. Lai, Synergistic multiple active species for the degradation of sulfamethoxazole by peroxymonosulfate in the presence of CuO@FeO_x@Fe-0, *Chem. Eng. J.*, 2020, **380**, 122568.

13 Y. P. Bao, W. D. Oh, T. T. Lim, R. Wang, R. D. Webster and X. Hu, Elucidation of stoichiometric efficiency, radical generation and transformation pathway during catalytic oxidation of sulfamethoxazole via peroxymonosulfate activation, *Water Res.*, 2019, **151**, 64-74.

14 F. Liu, H. Y. Zhou, Z. C. Pan, Y. Liu, G. Yao, Y. Guo and B. Lai, Degradation of sulfamethoxazole by cobalt-nickel powder composite catalyst coupled with peroxymonosulfate: Performance, degradation pathways and mechanistic consideration, *J. Hazard. Mater.*, 2020, **400**, 123322.

15 S. Z. Wang, L. J. Xu and J. L. Wang, Nitrogen-doped graphene as peroxymonosulfate activator and electron transfer mediator for the enhanced degradation of sulfamethoxazole, *Chem. Eng. J.*, 2019, **375**, 122041.

16 Y. S. Wang, Y. J. Song, N. Li, W. Liu, B. B. Yan, Y. Yu, L. Liang, G. Y. Chen, L. A. Hou and S. B. Wang, Tunable active sites on biogas digestate derived biochar for sulfanilamide degradation by peroxymonosulfate activation, *J. Hazard. Mater.*, 2022, **421**, 126794.

17 Y. Xu, S. Liu, M. Wang, J. Zhang, H. J. Ding, Y. Q. Song, Y. Zhu, Q. X. Pan, C. Zhao and H. P. Deng, Thiourea-assisted one-step fabrication of a novel nitrogen and sulfur co-doped biochar from nanocellulose as metal-free catalyst for efficient activation of peroxymonosulfate, *J. Hazard. Mater.*, 2021, **416**, 125796.

18 Y. L. Chen, X. Bai, Y. T. Ji and T. Shen, Reduced graphene oxide-supported hollow Co_3O_4@N-doped porous carbon as peroxymonosulfate activator for sulfamethoxazole degradation, *Chem. Eng. J.*, 2022, **430**, 132951.